

See discussions, stats, and author profiles for this publication at: <https://www.researchgate.net/publication/382890095>

Synthesis Method Comparison of N-Doped Carbons for Electrochemical Energy Storage

Article in ChemEngineering · August 2024

DOI: 10.3390/chemengineering8040080

CITATIONS
0

READS
29

5 authors, including:



Peteris Lesnicenoks
University of Latvia
99 PUBLICATIONS 150 CITATIONS

[SEE PROFILE](#)



Ainārs Knoks
University of Latvia
55 PUBLICATIONS 75 CITATIONS

[SEE PROFILE](#)



Virginija Vitola
University of Latvia
34 PUBLICATIONS 340 CITATIONS

[SEE PROFILE](#)



Janis Kleperis
University of Latvia
243 PUBLICATIONS 2,077 CITATIONS

[SEE PROFILE](#)

Article

Synthesis Method Comparison of N-Doped Carbons for Electrochemical Energy Storage

Roberts Palmbahs ^{1,2,*}, Peteris Lesnicenoks ^{1,2}, Ainars Knoks ^{1,*} , Virginija Vitola ¹  and Janis Kleperis ¹ 

¹ Institute of Solid State Physics, University of Latvia, LV-1063 Riga, Latvia; virginija.vitola@cfi.lu.lv (V.V.)

² Faculty of Natural Sciences and Technology, Riga Technical University, LV-1048 Riga, Latvia

* Correspondence: roberts.palmbahs@cfi.lu.lv (R.P.); ainars.knoks@cfi.lu.lv (A.K.)

Abstract: This study investigates nitrogen-doped carbon synthesis and electrochemical properties as electrode material for energy storage devices, an additional focus of the work is on the electrochemical exfoliation synthesis of nitrogen-doped carbon using various precursors and doping methods. The physical properties of the synthesized sample are characterized using X-ray photoelectron spectroscopy, scanning electron microscopy, and Raman spectroscopy. The electrochemical properties of the N-doped carbons are studied using cyclic voltammetry and galvanostatic charge-discharge cycling. Finally, the work explores the potential application of the N-doped carbons as electrode material for energy storage devices, such as supercapacitors. The results show that N-doped carbons exhibit electrochemical performance superior to that of graphene oxide, with higher electrical capacitance. The results demonstrate the potential of N-doped carbons as high-performance electrode materials for electrochemical energy storage applications. This paper aims to explain the advantages of N-doping in carbon materials more precisely in graphene and the use of these materials in creating electrodes for application in supercapacitors and batteries.

Keywords: carbon materials; electrochemical exfoliation; supercapacitors; graphene



Citation: Palmbahs, R.; Lesnicenoks, P.; Knoks, A.; Vitola, V.; Kleperis, J. Synthesis Method Comparison of N-Doped Carbons for Electrochemical Energy Storage. *ChemEngineering* **2024**, *8*, 80. <https://doi.org/10.3390/chemengineering8040080>

Academic Editor: Ştefan-Ovidiu Dima

Received: 26 March 2024

Revised: 11 July 2024

Accepted: 18 July 2024

Published: 5 August 2024



Copyright: © 2024 by the authors. Licensee MDPI, Basel, Switzerland. This article is an open access article distributed under the terms and conditions of the Creative Commons Attribution (CC BY) license (<https://creativecommons.org/licenses/by/4.0/>).

1. Introduction

This paper aims to investigate nitrogen-doped carbon synthesis and electrochemical properties as an electrode material for energy storage devices and to explain the electrochemical exfoliation process for the synthesis of N-functionalized graphene, along with the characterization of the acquired material for the intended purpose of energy storage. Considering the ever-increasing number of electrical devices currently in use, further sustainable and scalable developments in the energy storage sector are vital. Capacitors are excellent energy storage devices in fields where the longevity of the storage device is paramount, such as transportation, communications, entertainment, and many others. Capacitors could replace batteries in various everyday items that go through a lot of charge-discharge cycles during their use, such as but not limited to electric cars and cell phones. Batteries and their utilization pose a significant burden on the environment; finding an eco-friendly solution is an important goal to adhere to environmental goals by 2050. Graphene has already proven itself in many applications—energy, medicine, electronics, and food; it could be used more widely in electrical storage because of its unique set of physicochemical properties. Graphene-based capacitors would not only ensure a longer life span for battery-powered electronics but also reduce emissions for the weight of the energy storage device, as well as its biodegradability.

Doping graphene with nitrogen atoms enhances its electrochemical properties due to the transformation of graphene from a p-type conductor into an n-type conductor. The n-type semiconductor, unlike the p-type, conducts electricity due to an excess of electrons provided by the donor element, in this case, nitrogen, but the p-type semiconductor uses the lack of an electron, a hole, as the charge carrier for conductivity, such defects occur

when adding an acceptor element such as boron. Given the planar geometry of the nitrogen atom with a similar atomic size to carbon and nitrogen's five valence electrons, it can form strong covalent bonds with carbon atoms [1].

Nitrogen atoms can be added to graphene in various ways, and the atoms get incorporated into the graphene lattice with distinct types of bonds—pyridinic N, pyrrolic N, and quaternary or graphitic N [2–5]. In an XPS spectrum, N-doped graphene has an N1s band around 400 eV. The N1s spectral region is used to determine the types of bonds between nitrogen and carbon. Pyridinic N bond is observed at 399–400 eV, pyrrolic at 401–402 eV, graphitic at 402–403 eV, and various nitrogen oxide bonds at 408–410 eV [2,3,5–11]. A visual interpretation of the bonds can be seen in Figure 1.

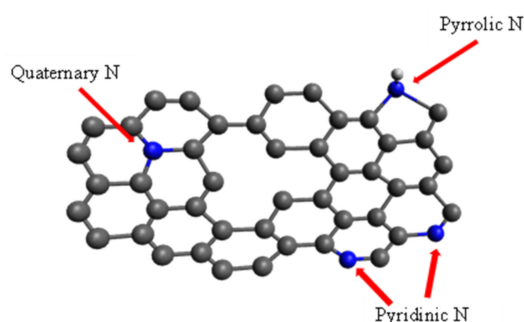


Figure 1. Common bonding configurations of Nitrogen-doped Graphene adapted from [12].

Carbon and activated carbon use in electrode development has been widely studied. Functionalizing graphene with different elements changes its electrochemical properties, thus opening/creating the possibility of obtaining several types of materials with a wide range of properties using one primary material—graphene. Nitrogen-doped few-layer graphene sheets (N-FLGS) are often used in electronics to make various devices. Currently, NG is used in the preparation of electrodes for batteries and supercapacitors, as well as for the production of electrically conductive ink, for which further applications are almost endless, for example, in gas sensing equipment, a catalyst for the electrocatalytic oxidation of methanol, is very topical [2,6,10,13–15].

Considering that supercapacitors have a higher cyclability than batteries, their use in electronic devices that require more charge-discharge cycles, such as phones, increases the longevity of the devices, thus reducing waste from discarding used batteries. Also, supercapacitors deliver energy faster without deteriorating at the same rate as batteries, which could be highly beneficial for use in starter motors or electric vehicles. The recycling process of carbon-based supercapacitors is shorter and more cost-effective [16–18] than that of batteries [19,20], which is essential not only considering the growing demand for energy storage devices and thus the amount of waste they produce but also for the security of the supply chain and production.

Taking into account the growing demand for electronic storage devices in industries such as transportation, where it is predicted that electric vehicles could account for two-thirds of all global vehicle sales by 2035 [21] or that the consumer electronics market grows every year with ever-increasing sales [22], it is fair to say that any advances in energy storage devices are useful in various industries. Although the devices fabricated during this study are yet to be commercially feasible, further research holds significant potential.

This work focuses on the functionalization of graphene with nitrogen using the electrochemical exfoliation method, while other methods, such as metal-organic frameworks, have also been successfully used for similar purposes [23–26]; this work focuses on the investigation of specific exfoliation as a quick and scalable method for functionalization and FLG production [27]. The synthesis of NG has been discussed previously [27]. In this work, additional materials were synthesized, and the main focus was the comparison of the materials and their electrochemical properties and applicability in supercapacitors.

2. Materials and Methods

Commercially available chemicals have been used. High-purity graphite rods (HOPG) (Alfa Aesar, Haverhill, MA, USA, 99.9995%), commercially available chemicals (analytical grade)— NaN_3 , NaNO_2 , HNO_3 , H_2SO_4 , citric acid, and carbamide were used as supplied without additional purification. Deionized water (conductivity 0.05 $\mu\text{S}/\text{cm}$) was used for electrolyte preparation and washing. Lithium hexafluorophosphate in ethylene carbonate and diethyl carbonate, 1.0 M LiPF_6 in EC/DEC = 50/50 (v/v), battery grade was used as the electrolyte, and polyvinylidene fluoride (PVDF) was used as the binder.

2.1. Material Synthesis

During this investigation, three materials were synthesized: nitrogen-doped graphene via exfoliation (NG), graphene oxide (GO), and carbon nanoparticles/quantum dots (CQD). In our previous work, we reported and demonstrated the exfoliation of NG [28]; the synthesis method in this work is similar. In this work, new materials have been added, and electrochemical properties for use in supercapacitors have been compared.

The functionalization of graphene with N atoms was accomplished through the electrochemical exfoliation of HOPG rods in nitrogen-rich electrolytes using a power supply. The synthesis was carried out in 800 mL beakers suspended in a water bath to cool the mixture as the process is exothermic; the schematic representation is shown in Figure 2. Exfoliation was carried out via impulse electrolysis, where the current was changed from 0 V to 10 V at 0.033 Hz. The synthesis process was optimized to the highest efficiency, which was for 20 h; shortening or lengthening the time of the process results in an inferior electrode exfoliation and a noticeable loss of process efficiency with regards to the material yield.

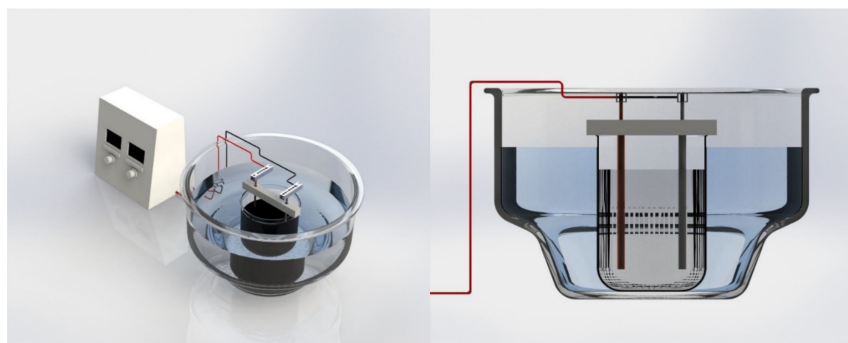


Figure 2. Schematic representation of the reactor.

Two nitrogen-rich electrolytes for N-doping were used: 1M NaN_3 and 1M NaNO_2 with the addition of 75 mL of HNO_3 to the 500 mL volume. Exfoliation is carried out as described above. The same exfoliation setup produced GO by substituting N-rich electrolyte with 1M H_2SO_4 , also optimized for the highest material yield.

The methods were chosen due to their low raw material, and synthesis power demands compared to other methods such as CVD, plasma—treatment, annealing processes, adsorption, and others. Thus, the method in itself provides a lower production cost [9,10,14]. In addition, the electrochemical exfoliation method of doping graphene offers a high level of N-doping [3], especially using a nitrogen-rich precursor such as sodium azide, which can functionalize graphene as it easily decomposes in ions. Other methods of N-doped graphene production have been more widely researched.

Carbon quantum dots (CQD) were synthesized via microwave synthesis. A 1:1 mass ratio aqueous solution with citric acid and urea was prepared, and 100 mL of the resulting mixture was placed in a SynthWAVE microwave synthesis system (Milestone, Sorisole, Italy) in a 1 L Teflon reactor. Synthesis was performed under an argon atmosphere to ensure that airborne substances did not contaminate the sample. The microwave was set to 1250 W for solution irradiation. The synthesis continued for 2 min until all the solution evaporated,

and the formation of a black mass was visually observed in the reactor. The CQD presence was confirmed by luminescence emission spectrum measurement shown in Figure 3.

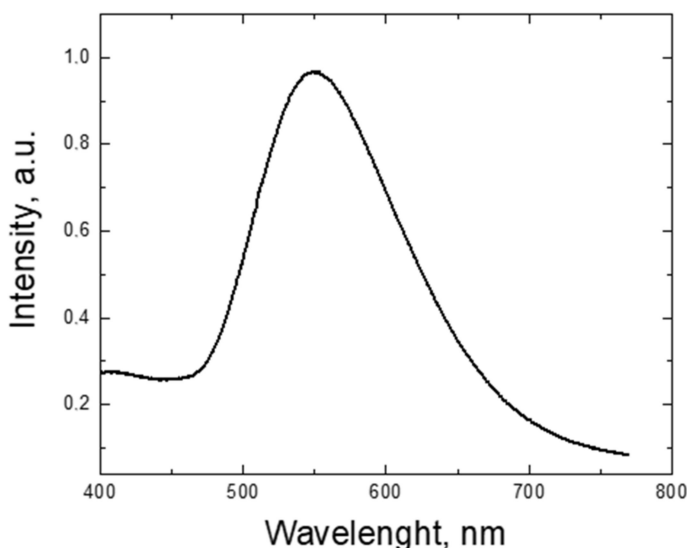


Figure 3. The luminescence emission measurement of the CQD sample was excited with a 266 nm YAG laser and measured with an ANDOR iDUS spectrometer (Oxford Instruments, Abingdon, UK) coupled with a CCD camera.

All obtained materials were later dispersed using a UP200St ultrasonic homogenizer (Hielscher, Teltow, Germany), filtered through 1, 0.45, 0.2, and 0.1 μm filters, and washed with 1L deionized water.

2.2. Material Characterization Methods

To measure the XPS spectra, an XPS (ESCALAB 250 Xi, Thermo Scientific, Waltham, MA, USA) hemispherical analyzer was operated at 20 eV pass and using Al-K α radiation with an overall resolution of approximately 0.45 eV. SEM images were obtained using Thermo Scientific™ Helios™ 5 UX operated at 20.00 kV electron acceleration and 50 pA current. Raman spectra were measured in backscattering configuration by Andor Shamrock 303 spectrograph with 1200 L/mm grating and cooled silicon CCD, using 532.08 nm 200 mW continuous wave (CW) excitation. The spectral resolution was 0.7 nm ($\approx 20 \text{ cm}^{-1}$) FWHM (full width at half maximum). Interference by sample background luminescence was mitigated by its partial photobleaching; the Raman spectrum was obtained as the non-bleachable component of the as-measured composite PL-Raman spectrum.

2.3. Development of Electrodes

The materials obtained were suspended in N-methyl-2-pyrrolidone (NMP), and polyvinylidene fluoride (PVDF) was added to these solutions as a binder in the following proportions. 5 wt% PVDF was added to NaN_3 and NaNO_2 synthesized NG, as well as GO, while 10 wt% PVDF was added to CQD. The resulting mixtures were sonicated using a UP200St ultrasonic homogenizer to obtain a more uniform dispersion. The obtained inks were applied to aluminum foil using Doctor blade coating and dried in a drying oven for 3 h.

A press was used to obtain electrodes of favorable size ($d = 12 \text{ mm}$). The electrodes were placed in a vacuum oven for 2 h at 120 °C and in the glovebox's antechamber to remove excess moisture.

The supercapacitors were assembled in a glove box using Swagelok battery cells, as seen in Figure 4. The electrodes were separated with a Whatman glass microfiber separator (Sigma Aldrich, St. Louis, MO, USA) that was saturated with 300 μL of LiPF_6 electrolyte.



Figure 4. Swagelok battery cell.

Electrical measurements were performed using an Autolab PGSTAT302N Potentiostat-Galvanostat (Metrohm Autolab, Utrecht, The Netherlands).

3. Results and Discussion

In the synthesis process of N-functionalized graphene and graphene oxide, observable changes in the electrolyte color from transparent to grey and eventually opaque black signify successful exfoliation, confirming the production of NG or graphene from graphite electrodes. Initial stages of electrolysis presumably involve the decomposition of azide and sodium nitrite, releasing Na^+ , N^{3-} , and NO^{2-} ions. This claim is supported by the X-ray diffraction (XRD) data presented in our previous work [14] and the X-ray photoelectron spectroscopy (XPS) data, complemented by findings reported in [29].

The proposed reaction mechanisms are as follows:

Decomposition of azide ion to nitrogen (Equation (1)):



Interaction of azide ion with water (Equation (2)):

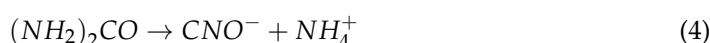


Nitrite ions are disproportionate, yielding nitric ions and nitric oxide through the following reaction (Equation (3)):



The decomposition and reactions of N^{3-} and NO^{2-} ions are hypothesized to promote the intercalation within graphite rods, facilitating the separation of graphite layers to form N-MLG and N-FLGS. Concurrently, the production of N_2 , NH_3 , and potentially O_2 could contribute to further exfoliation and functionalization of the material with nitrogen and oxygen groups.

During the synthesis of carbon quantum dots, the reaction between citric acid and carbamide in an aqueous solution initially results in a black solid. Upon dispersion in water, this material imparts a yellowish tint and exhibits green fluorescence under blue light, indicating the successful formation of graphene oxide, which is subsequently nitrogen-functionalized by carbamide. The decomposition of carbamide is represented by (Equation (4)):



The resulting cyanate ion transforms into CO_2 and ammonia, further functionalizing the material.

While consistent with the available literature [30,31], these proposed mechanisms are based on interpretative analysis of experimental outcomes. Future work involving direct experimental validation is planned.

3.1. Scanning Electron Microscopy of the Materials

Figure 5 shows SEM images of N-functionalized graphene formed by exfoliating graphite electrodes in 1M Na₃N solution. In picture Figure 5A, the graphene plates created as a result of exfoliation can be seen; they are 0.3–1.2 µm long and 10–15 nm thick. In the image Figure 5B, it is possible to observe larger (100–400 nm) particles and generally small and hardly visible 7–15 nm graphene particles clustered together in the middle. In parts Figure 5C,D of the picture, it is possible to observe graphene particles of different sizes, primarily µm-sized plates and grains, as well as barely visible nm-sized grains.

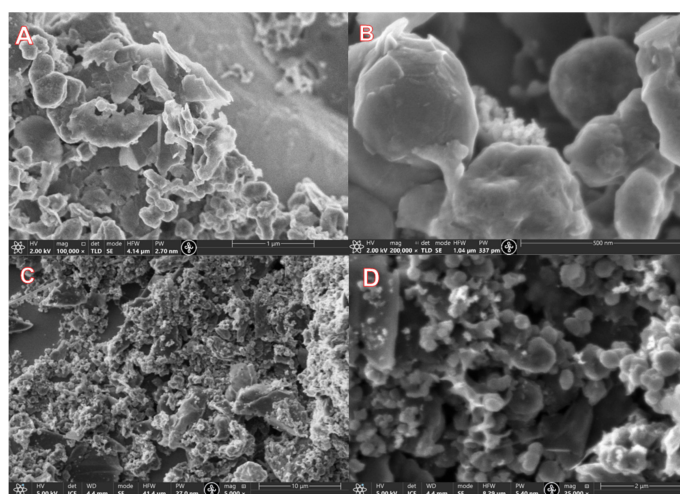


Figure 5. Helios 5UX SEM images of sample NG_NaN₃. (A) Thick graphene plates (B) smaller fraction of the thick plates (C) lower magnification graphene particle (D) High magnification of graphene particles.

Figure 6 shows SEM images of NG formed by exfoliating graphite electrodes in 1M NaNO₂ solution. In part Figure 6A of the picture, 100–400 nm thick graphene plates of varied sizes, which have not entirely separated from each other during the exfoliation process, can be observed. In part Figure 6B, it is possible to observe a similar situation at a smaller magnification—the thickness of the plates is approximately 200–300 nm. The graphene shown in Figure 6A,B was suspended in NMP solvent, and 5% PVDF was added to the mixture. It is possible that the graphene plate formations in Figure 6A,B were formed during ink drying rather than indicating synthesis failure. In parts Figure 6C,D, it is possible to observe graphene particles of various sizes ranging from 0.2–4 µm.

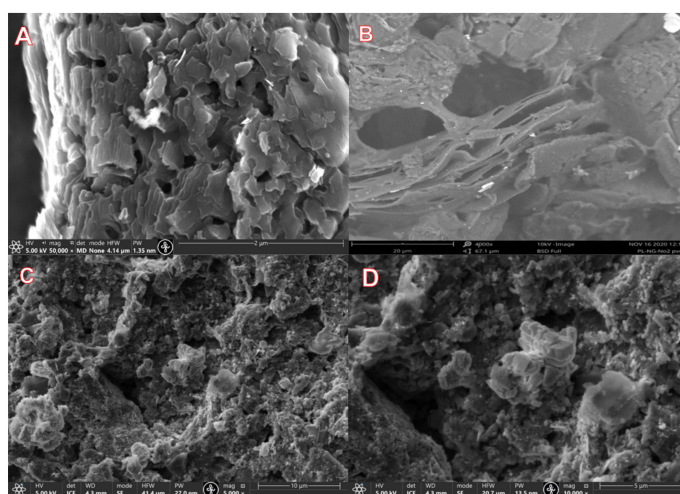


Figure 6. Helios 5UX (A–C) and Phenom Pro (D) SEM images of sample NG_NaNO₂.

Figure 7 shows SEM images of graphene oxide obtained by exfoliating HOPG electrodes in concentrated sulfuric acid. In part Figure 7A of the picture, it is possible to observe GO plates of different sizes (1–10 μm). The edges of the graphene oxide plates are visible, although the specific magnification is not high enough to judge the thickness of the plates. In part Figure 7B of the picture, we see a close-up of the previous image. Both large (1–4 μm) and small (150–400 nm) plates and particles agglomerated on each other can be observed. It is also possible to observe multi-plate facets of approximate size (20–80 nm).

In part Figure 7C of the image, at the highest magnification, it is already possible to observe not only plates of the previously seen size (150–400 nm) but also small size (approximately 15–40 nm) particles. In this part of the image, some edges of the graphene plates can also be seen, indicating that the thicknesses of the plates in the given area are of varied sizes (approximately 13–55 nm). In part Figure 7D of the image, large graphene oxide plates can be observed in varied sizes from smaller (200–700 nm) to larger (1–9 μm) graphene oxide particles.

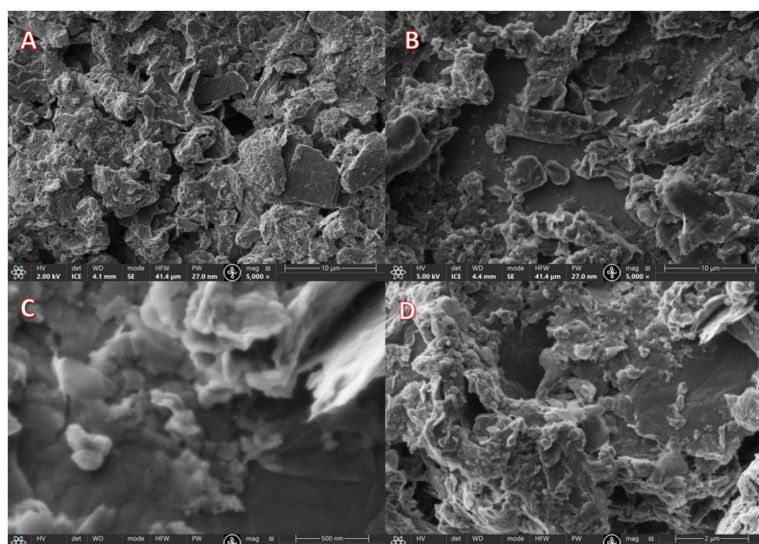


Figure 7. Helios 5UX SEM images of sample GO. (A) various sized GO plates (B) Greater magnification of GO plates (C) highest magnification showing 150–400 nm and smaller particles (D) Large GO plates are visible.

Several types of complications occurred during the SEM measurements of the CQD sample. Although the material was deposited on a Si substrate according to the same principle as the other samples, it produced a uniform coating, making it challenging to observe a large number of particles of different sizes in the sample. Figure 8 shows SEM images of this relatively uniform coating. Compared to other images where it is possible to see several individual plates, particles, and agglomerates, these images show a cracked but relatively smooth surface.

This type of layer apparently formed because small particles were obtained during the synthesis process, which resulted in a distinct uniform dispersion. All particles settled equally quickly on the Si surface during the application process.

Pore size approximation was done with Python software (Python 3.9), using SEM images with OpenCV library for image processing and sci-kit-image library for image analysis. This reveals that NG_NaN₃, NG_NaN₃, and GO samples contain pores ranging from 50 nm to 300 nm diameter, the median value of NG_NaN₃ being 120 nm, NG_NaN₃—74 nm and GO—68 nm.

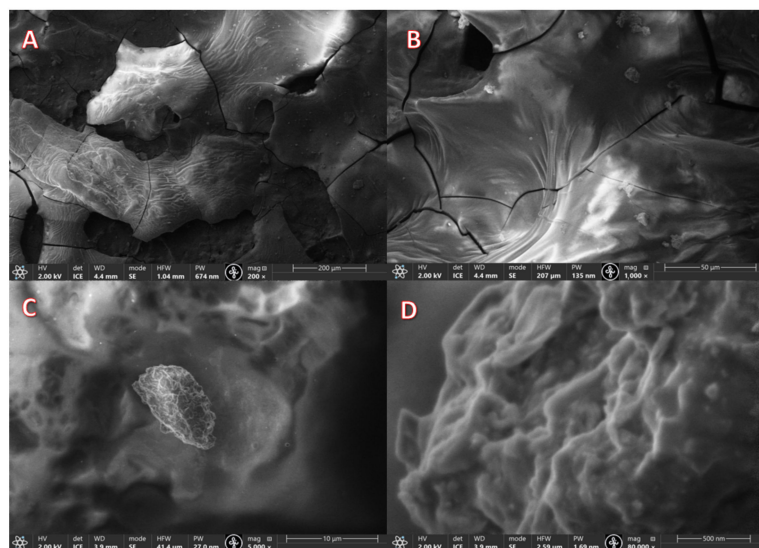


Figure 8. Helios 5UX SEM images of sample CQD. (A) Uniform coating of the sample (B) Larger magnification of the coating (C) Single particle agglomerate (D) Higher magnification of the particle.

AFM measurements were also performed on the CQD sample, which revealed that particles no larger than 17 nm were observed in a well-dispersed sample (Figure 9).

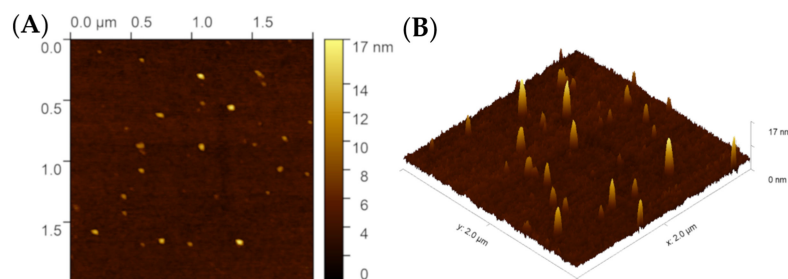


Figure 9. (A) 2D and (B) 3D AFM measurement for CQD sample.

3.2. X-ray Photoelectron Spectroscopy of Samples

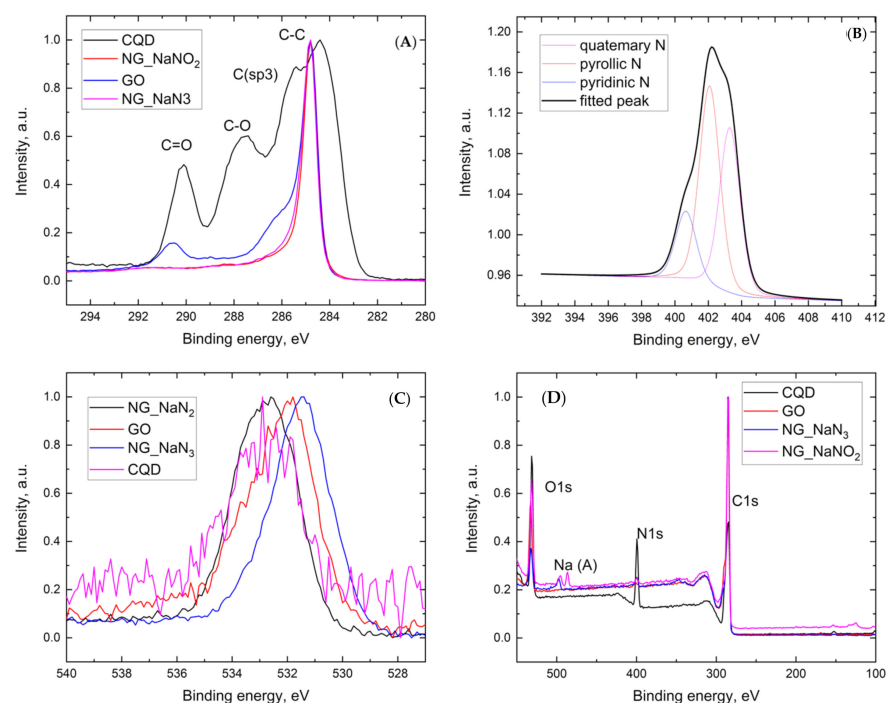
XPS survey spectra were taken for all materials in order to obtain quantification data. Table 1. represents the quantification data gathered in the XPS measurements. All of the materials present a high amount of carbon as expected, as well as oxygen and nitrogen, which were present in the synthesis process. The GO and CQD samples show a high fluorine content, which could be explained by contamination during the synthesis process or the contamination of raw materials. The CQD sample presents a significantly high nitrogen and oxygen content, which is expected due to the high content of these atoms in raw materials used in synthesis.

The NG samples contain many contaminants such as Na, Sn, and Cu that could have resulted from impure graphite rods being used in the synthesis or the synthesis electrolyte gaining contact with the prongs connecting the power supply to the graphite rods, as seen in Figure 2; this could have led to the contamination. Nonetheless, it can be determined that using an aqueous sodium azide electrolyte produces a material with a lower oxygen but a higher nitrogen content compared to using an aqueous sodium nitrate electrolyte.

As seen in Figure 10A, the C1s region of the XPS scan has distinct peaks at 284 eV, 285 eV, 286 eV, and 290 eV. These peaks indicate the presence of C-C, sp^3 hybridized carbon, C-O, and C=O bonds, respectively. The NG_NaN₃ and NG_NaNO₂ samples seem to contain only C-C bonds, which is expected in functionalized graphene XPS spectrum. The GO sample scan shows more C=O and C-O bonds as expected in graphene oxide.

Table 1. XPS quantification data.

GO	
Name	Atomic %
C	72.69
F	15.43
O	10.83
N	0.76
S	0.29
CQD	
Name	Atomic %
C	53.79
F	16.87
O	16.25
N	12.38
Si	0.71
NG_NaNO ₂	
Name	Atomic %
C	79.42
Cu	3.53
O	14.09
N	1.6
Si	0.78
Na	0.4
Sn	0.19
NG_NaN ₃	
Name	Atomic %
C	88.94
O	6.47
N	2.53
Na	1.32
Si	0.52

**Figure 10.** XPS scans: (A) C1s band of the XPS spectrum (narrow scan), (B) N1s band of sample NG_NaN₃ XPS spectrum (narrow scan), (C) O1s band of the XPS spectrum (narrow scan), and (D) XPS survey spectra of synthesized samples.

In Figure 10B, the colored lines are the deconvolution of peaks, the black line is a fitted peak, and the dashed line is the XPS data. Figure 10B shows the N1s band of the XPS spectrum taken for N-functionalized graphene synthesized in sodium azide. Deconvolution of the spectrum reveals peaks at 400.5, 402.5, and 403.5 eV, indicating the presence of pyridinic, pyrrolic, and quaternary nitrogen in the obtained material.

The O1s spectra indicate the presence of C-O-C (532.6 eV) bonds in CQD and NG_NaN₃ samples, and C-O (531.8 eV) bands in GO and NG_NaNO₃ samples [32,33].

3.3. Raman Spectroscopy of Graphene

Graphite and graphene have six vibrational modes: 2E_{2g}, 2B_{2g}, E_{1u}, and A_{2u}, as described [34]. The E_{2g} modes are Raman active, and the first mode produces a band at 42 cm⁻¹ in the Raman spectrum that is not usually observable. The other E_{2g} mode gives rise to the G band at 1582 cm⁻¹.

In a perfect Raman spectrum, the G band, observed around 1582 cm⁻¹, is the leading band in many Raman spectra of materials where the carbon atoms are in the sp² hybridization state. The G band is produced by the center of a doubly degenerate zone in the E_{2g} mode [34,35].

The D band, observed around 1350 cm⁻¹, arises from the so-called breathing problems of the hexagonal carbon structure (the carbon atoms in the hexagonal structure move away from the center of the structure under the influence of interatomic energy). This band can be observed in the spectrum when activated by a defect in the obtained carbon material or mechanically generated defects, functionalization-generated defects, oxidation defects, etc. Activations are also carried out by the double resonance of this mode [34–37].

The double resonance charge activates phonons with a small electric charge (q), this process results in the D' band around 1620 cm⁻¹, indicating defects in the carbon material. The D+D' band at 2970 cm⁻¹ is a combination of the D and D' bands, so a saturated defect is required for the carbon material to reach the observer spectrum. The D+D'' band observed around 2450 cm⁻¹ is a graphite band that can be observed in carbon materials with defects.

The 2D band is the overtone of the D and D' bands observed around 2700 cm⁻¹. Clearly, from the D and D' bands, the 2D band is also possible for the observer in defect-free materials, as the bands of its occurrence are the same. But the 2D band does not require activation, to be observed in the Raman spectrum [34–37].

Samples show high mutual similarity in the Raman spectra such as classical graphite bands—G, D, 2D and D+D'' can be observed in Figure 11. In all cases, the highest intensity is precisely for the G band, which is expected since it is the most characteristic band in the materials containing sp² hybridized carbon atoms.

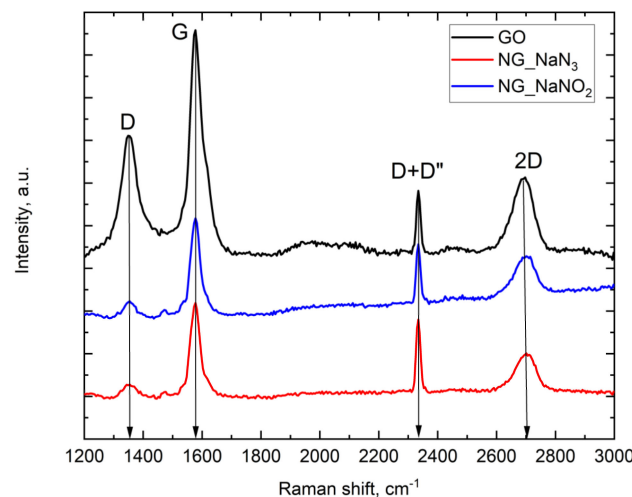


Figure 11. Raman spectrum for NG_NaNO₂, NG_NaN₃, and GO samples.

As seen in Figure 11, the G band reaches its maximum at 1577 cm^{-1} , indicating a more significant number of graphene layers; if the material contained more monolayer graphene, then the band would shift closer to 1587 cm^{-1} [37]. However, it is also mentioned that temperature, functionalization of the material, and other factors affect the location of this band. Given that N-functionalized graphene and graphene oxide were obtained, the intensity of the G band provides information about the number of graphene layers. Considering the high intensities in the obtained spectra, it is possible to conclude that multilayer graphene has been obtained.

The D bands in all spectra peak at 1354 cm^{-1} . Although the position of the band does not provide much information about the properties of the material, its intensity indicates the number of defects in the obtained samples [34]. When proportionally comparing the D band with other bands in all obtained spectra, we observe that in the graphene oxide sample, this band is significantly more intense than in both N-functionalized graphene samples, which would indicate that the obtained graphene oxide has more surface and structural defects than the NG samples. Such a result is also expected since graphene oxide serves as a starting material in various syntheses due to its high number of defects; as example, it is possible to cite plasma treatment for the production of N-functionalized graphene [37].

3.4. Electrochemical Measurements

Electrical measurements were performed using an Autolab PGSTAT302N Potentiostat-Galvanostat. Cyclic voltammetry and charge/discharge kinetics data were obtained for the assembled supercapacitors.

Figure 12 shows the cyclic voltammograms of capacitors with electrodes containing GO, CQD, NG_NaN₃, and NG_NaNO₂ samples, respectively, showing the current ratio against the applied electric potential.

Figure 12 shows that the cyclic voltammetry graphs tend to take the shape (rectangle), as described in the literature sources [38–41], although it seems that the graphs are narrower, which indicates the occurrence of resistance in the system. Resistance can be caused by the binder added to the material during the development of electrodes, as mentioned by Xintong Ren et al. [42], or by something as simple as insufficient wetting of the separator during supercapacitor assembly, or due to the electron transport characteristics of electrode materials.

Considering that the data indicate a strong consistency of the results during the charge/discharge process, it can be concluded that functional capacitors have been obtained. However, their efficiency can be significantly improved. The most stable cyclability is observed for the capacitor containing the graphene oxide sample, and the highest degradation is observed for the capacitor containing the N-functionalized graphene synthesized in sodium azide.

Figure 12 shows charge/discharge kinetics graphs of capacitors whose electrodes were developed using GO, CQD, NG_NaN₃, and NG_NaNO₂ samples, respectively, where the current and the applied electric potential are shown over time. The electric current curve should be symmetric for an ideal capacitor and resemble the electric potential graph. As seen in all graphs, there is an observable deviation from the ideal state, although all graphs tend to take this form. The graphene oxide sample most closely mimics the ideal case described in the literature. Deviations from the ideal form are formed due to various resistances: for example, the choice of binder, separator, electrolyte, and other factors [43].

The differences in sample voltages are due to the surface properties of the coating.

The cyclic voltammogram graph of a capacitor resembles that of a rectangle, as seen in Figure 12. A commercial capacitor with known parameters was taken and evaluated using methods with adjusted parameters (using higher voltages specified by the manufacturer) that better fit the specific device. As it can be observed the shape of the graph is rectangular and some degradation can be observed that could be explained by some connection issues because the graph evens out and resembles that of the theoretical capacitor.

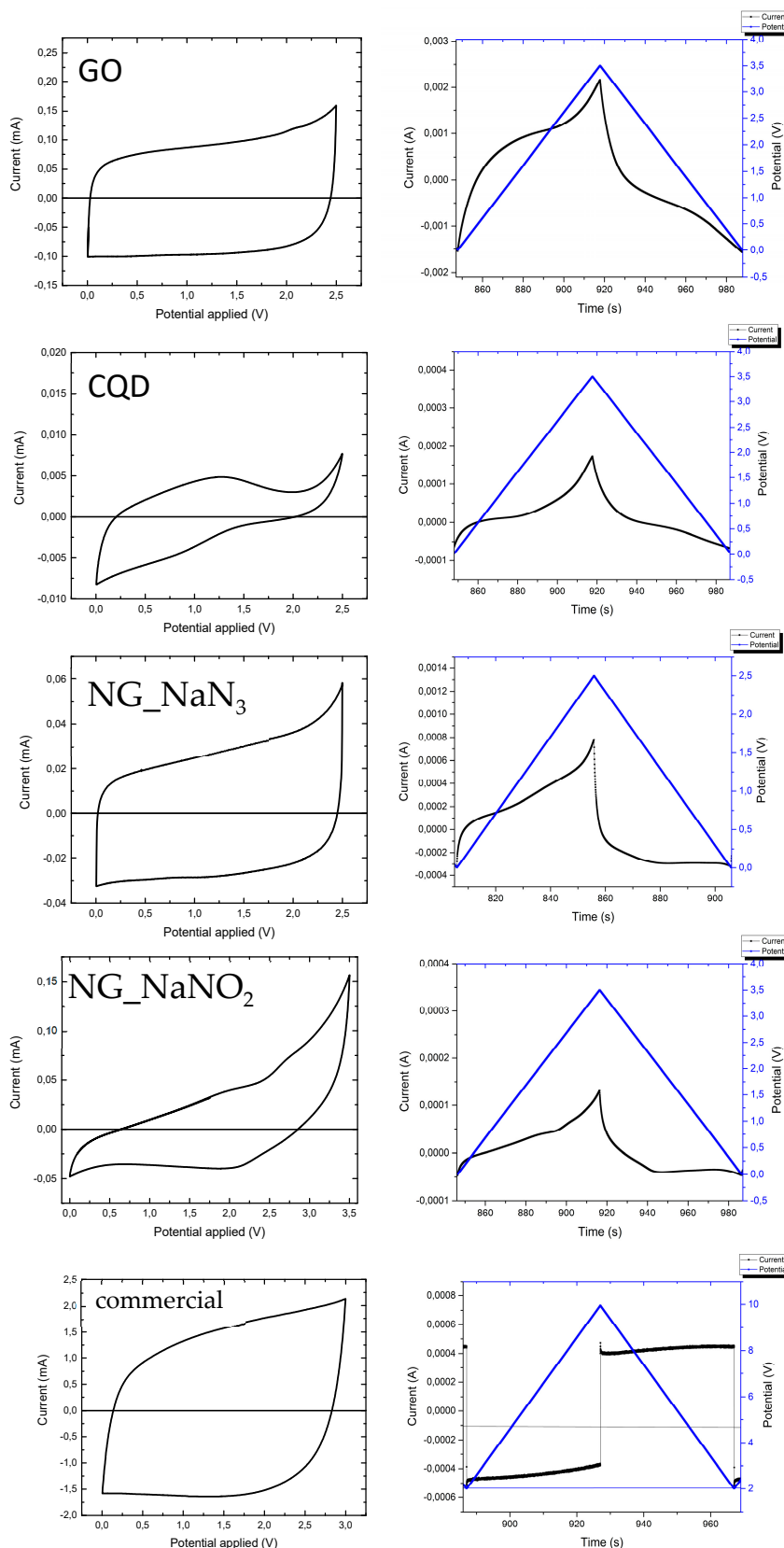


Figure 12. Cyclic voltammogram of the samples (left) and charge/discharge kinetics of respective sample (right).

During the measurements, the total electrical charge flowing through the supercapacitor was also recorded. Using this data, the electrical capacity of the material was calculated

(Table 2). The formulas used in capacity calculations can be found in: [44,45]. The capacity is comparable to those reported in [44]; it is noteworthy that CQD, as seen in Figure 9, have been successfully used in printed triboelectric nanogenerators providing stabilization [46], on the other hand, as we can see here, CQD as standalone material for energy storage device shows less promise in comparison to alternatives as NG_NaN₃. Thus, material, synthesis and parameters can be determining specific use-case.

Table 2. Electrical capacity of the samples.

Sample Name	m(g)	Capacity/Mass (F/g)
GO	0.0070	41
CQD	0.0074	38
NG_NaNO ₂	0.0065	44
NG_NaN ₃	0.0044	64
Commercial capacitor	0.0059	57

4. Conclusions

The synthesis of N-functionalized graphene and graphene oxide was successfully completed using the electrochemical exfoliation method in different electrolyte solutions that served as the nitrogen and oxygen precursors. In addition, carbon quantum dots were obtained using a microwave synthesis method.

The physical properties of synthesized materials were investigated, and it was concluded that graphene and carbon quantum dots were synthesized as confirmed by XPS and Raman analysis. In the case of N-doped graphene, it was concluded that sodium azide is a viable nitrogen source as it does not contain various elements that would bond with the graphene impeding its electrochemical properties. As seen in the XPS data, the azide provided a higher nitrogen and lower oxygen content in the material.

The electrochemical measurements show that all obtained materials work as capacitors, but improvements are necessary to gain the quality on par with commercially available products. The obtained capacitors show promise in the form of cyclability, as seen by two of the four samples showed insignificant amounts of degradation. The electrical capacitance of the tested commercial capacitor was 0.001 F, and the capacitors containing the synthesized material showed a capacitance of up to 0.3866 F, indicating that the obtained material can potentially store more electric charge than the commercially available capacitor.

Further research is required to strengthen the aforementioned claims and to scale up the synthesis for commercial use. Studies should be carried out to achieve a better understanding of the characteristics that each nitrogen bond type provides to the material to ascertain how to maximize desired electrochemical properties such as capacitance.

Author Contributions: R.P.: conceptualization, methodology, formal analysis, investigation, resources, data curation, writing—original draft, visualization. A.K.: conceptualization, formal analysis, writing—review & editing, supervision, project administration, funding acquisition. P.L.: conceptualization, formal analysis, writing—review & editing. V.V.: formal analysis, investigation, data curation, writing—review & editing. J.K.: conceptualization, writing—review & editing, funding acquisition. All authors have read and agreed to the published version of the manuscript.

Funding: Thanks are provided for the financial support from the Latvian Science Council project LZP FLPP No. LZP-2018/1-0194 and Virginija Vitola acknowledge the project LZP-2023/1-0521. Authors acknowledges the Institute of Solid State Physics of the University of Latvia, which as a center of excellence has received funding from the European Union framework program Horizon 2020 H2020-WIDESPREAD-01-2026-2017-TeamingPhase2 within the framework of grant agreement No. 739508 of the CAMART2 project.

Data Availability Statement: Data is available upon personal requests. I hope that is acceptable. The data generated in this study will be made available upon reasonable request.

Acknowledgments: Ainars Knoks and Peteris Lesnicenoks for the invested work, time, and patience, as well as Janis Kleperis for valuable advice. We also thank ISSP UL colleagues for their support during the development of the work, especially Virginija Vitola for XPS and Raman data acquisition, Liga Ignatane for help in obtaining SEM images using the Helios 5UX electron microscope, Paulis Gurdziels for assistance in developing the synthesis device electronics, and Raitis Sika for the computer model of the synthesis device.

Conflicts of Interest: The authors declare no conflicts of interest.

References

1. Fan, M.; Feng, Z.-Q.; Zhu, C.; Chen, X.; Chen, C.; Yang, J.; Sun, D. Recent progress in 2D or 3D N-doped graphene synthesis and the characterizations, properties, and modulations of N species. *J. Mater. Sci.* **2016**, *51*, 10323–10349. [[CrossRef](#)]
2. Bundaleska, N.; Henriques, J.; Abrashev, M.; Botelho do Rego, A.M.; Ferraria, A.M.; Almeida, A.; Dias, F.M.; Valcheva, E.; Arnaudov, B.; Upadhyay, K.K.; et al. Large-scale synthesis of free-standing N-doped graphene using microwave plasma. *Sci. Rep.* **2018**, *8*, 12595. [[CrossRef](#)] [[PubMed](#)]
3. Yang, Y.; Shi, W.; Zhang, R.; Luan, C.; Zeng, Q.; Wang, C.; Li, S.; Huang, Z.; Liao, H.; Ji, X. Electrochemical Exfoliation of Graphite into Nitrogen-doped Graphene in Glycine Solution and its Energy Storage Properties. *Electrochim. Acta* **2016**, *204*, 100–107. [[CrossRef](#)]
4. Usachov, D.; Vilkov, O.; Grüneis, A.; Haberer, D.; Fedorov, A.; Adamchuk, V.K.; Preobrajenski, A.B.; Dudin, P.; Barinov, A.; Oehzelt, M.; et al. Nitrogen-Doped Graphene: Efficient Growth, Structure, and Electronic Properties. *Nano Lett.* **2011**, *11*, 5401–5407. [[CrossRef](#)] [[PubMed](#)]
5. Maddi, C.; Bourquard, F.; Barnier, V.; Avila, J.; Asensio, M.-C.; Tite, T.; Donnet, C.; Garrelie, F. Nano-Architecture of nitrogen-doped graphene films synthesized from a solid CN source. *Sci. Rep.* **2018**, *8*, 3247. [[CrossRef](#)]
6. Xiong, B.; Zhou, Y.; Zhao, Y.; Wang, J.; Chen, X.; O'Hayre, R.; Shao, Z. The use of nitrogen-doped graphene supporting Pt nanoparticles as a catalyst for methanol electrocatalytic oxidation. *Carbon* **2013**, *52*, 181–192. [[CrossRef](#)]
7. Ma, R.; Ren, X.; Xia, B.Y.; Zhou, Y.; Sun, C.; Liu, Q.; Liu, J.; Wang, J. Novel synthesis of N-doped graphene as an efficient electrocatalyst towards oxygen reduction. *Nano Res.* **2016**, *9*, 808–819. [[CrossRef](#)]
8. Carrillo-Rodríguez, J.C.; Alonso-Lemus, I.L.; Siller-Ceniceros, A.A.; Pizá-Ruiz, P.; Vargas-Gutiérrez, G.; Rodríguez-Varela, F.J. Easy synthesis of N-doped graphene by milling exfoliation with electrocatalytic activity towards the Oxygen Reduction Reaction (ORR). *Int. J. Hydrogen Energy* **2017**, *42*, 30383–30388. [[CrossRef](#)]
9. Xu, H.; Ma, L.; Jin, Z. Nitrogen-doped graphene: Synthesis, characterizations and energy applications. *J. Energy Chem.* **2018**, *27*, 146–160. [[CrossRef](#)]
10. Yadav, R.; Dixit, C. Synthesis, characterization and prospective applications of nitrogen-doped graphene: A short review. *J. Sci. Adv. Mater. Devices* **2017**, *2*, 141–149. [[CrossRef](#)]
11. Fan, M.; Zhu, C.; Yang, J.; Sun, D. Facile self-assembly N-doped graphene quantum dots/graphene for oxygen reduction reaction. *Electrochim. Acta* **2016**, *216*, 102–109. [[CrossRef](#)]
12. Granzier-Nakajima, T.; Fujisawa, K.; Anil, V.; Terrones, M.; Yeh, Y.-T. Controlling Nitrogen Doping in Graphene with Atomic Precision: Synthesis and Characterization. *Nanomaterials* **2019**, *9*, 425. [[CrossRef](#)] [[PubMed](#)]
13. Şenel, B.; Demir, N.; Büyükköroğlu, G.; Yıldız, M. Graphene quantum dots: Synthesis, characterization, cell viability, genotoxicity for biomedical applications. *Saudi Pharm. J.* **2019**, *27*, 846–858. [[CrossRef](#)]
14. Yu, P.; Lowe, S.E.; Simon, G.P.; Zhong, Y.L. Electrochemical exfoliation of graphite and production of functional graphene. *Curr. Opin. Colloid Interface Sci.* **2015**, *20*, 329–338. [[CrossRef](#)]
15. Khan, F.; Baek, S.-H.; Kim, J.H. Preparation Method of Reduced and N-Doped Graphene Oxide and the Reduced and N-Doped Graphene Oxide Thereby. US 2016/0315194 A1, 27 October 2016. Available online: <https://worldwide.espacenet.com/patent/search/family/057146912/publication/US2016315194A1?q=pn=US2016315194A1> (accessed on 30 October 2020).
16. Chodankar, N.R.; Patil, S.J.; Hwang, S.-K.; Shinde, P.A.; Karekar, S.V.; Raju, G.S.R.; Ranjith, K.S.; Olabi, A.G.; Dubal, D.P.; Huh, Y.S.; et al. Refurbished carbon materials from waste supercapacitors as industrial-grade electrodes: Empowering electronic waste. *Energy Storage Mater.* **2022**, *49*, 564–574. [[CrossRef](#)]
17. Yanshyna, O.; Weissman, H.; Rybtchinski, B. Recyclable electrochemical supercapacitors based on carbon nanotubes and organic nanocrystals. *Nanoscale* **2020**, *12*, 8909–8914. [[CrossRef](#)] [[PubMed](#)]
18. Jiang, G.; Pickering, S.J. Recycling supercapacitors based on shredding and mild thermal treatment. *Waste Manag.* **2016**, *48*, 465–470. [[CrossRef](#)]
19. Fan, E.; Li, L.; Wang, Z.; Lin, J.; Huang, Y.; Yao, Y.; Chen, R.; Wu, F. Sustainable Recycling Technology for Li-Ion Batteries and Beyond: Challenges and Future Prospects. *Chem. Rev.* **2020**, *120*, 7020–7063. [[CrossRef](#)]
20. Neumann, J.; Petranikova, M.; Meeus, M.; Gamarra, J.D.; Younesi, R.; Winter, M.; Nowak, S. Recycling of Lithium-Ion Batteries—Current State of the Art, Circular Economy, and Next Generation Recycling. *Adv. Energy Mater.* **2022**, *12*, 2102917. [[CrossRef](#)]
21. EV-Volumes—The Electric Vehicle World Sales Database. Available online: <https://www.ev-volumes.com/> (accessed on 17 January 2024).

22. Consumer Electronics Market Size to Surpass US\$ 1264.52 Billion by 2032. Available online: <https://www.precendenceresearch.com/consumer-electronics-market> (accessed on 17 January 2024).
23. Shi, Y.; Zhu, B.; Guo, X.; Li, W.; Ma, W.; Wu, X.; Pang, H. MOF-derived metal sulfides for electrochemical energy applications. *Energy Storage Mater.* **2022**, *51*, 840–872. [CrossRef]
24. Xu, Y.; Tu, W.; Zhang, B.; Yin, S.; Huang, Y.; Kraft, M.; Xu, R. Nickel Nanoparticles Encapsulated in Few-Layer Nitrogen-Doped Graphene Derived from Metal–Organic Frameworks as Efficient Bifunctional Electrocatalysts for Overall Water Splitting. *Adv. Mater.* **2017**, *29*, 1605957. [CrossRef] [PubMed]
25. Kim, M.; Xin, R.; Earnshaw, J.; Tang, J.; Hill, J.P.; Ashok, A.; Nanjundan, A.K.; Kim, J.; Young, C.; Sugahara, Y.; et al. MOF-derived nanoporous carbons with diverse tunable nanoarchitectures. *Nat. Protocols* **2022**, *17*, 2990–3027. [CrossRef] [PubMed]
26. Li, Q.; Xia, Y.; Wan, X.; Yang, S.; Cai, Z.; Ye, Y.; Li, G. Morphology-dependent MnO₂/nitrogen-doped graphene nanocomposites for simultaneous detection of trace dopamine and uric acid. *Mater. Sci. Eng. C* **2020**, *109*, 110615. [CrossRef] [PubMed]
27. Amiri, A.; Naraghi, M.; Ahmadi, G.; Soleymaniha, M.; Shanbedi, M. A review on liquid-phase exfoliation for scalable production of pure graphene, wrinkled, crumpled and functionalized graphene and challenges. *FlatChem* **2018**, *8*, 40–71. [CrossRef]
28. Olins, R.; Lesnicenoks, P.; Kleperis, J.; Knoks, A.; Lukosevics, I. Electrochemical exfoliation-streamline method for synthesis of nitrogen doped graphene. *Chemija* **2021**, *32*, 9–16. [CrossRef]
29. Ferrari, A.C.; Meyer, J.C.; Scardaci, V.; Casiraghi, C.; Lazzeri, M.; Mauri, F.; Piscanec, S.; Jiang, D.; Novoselov, K.S.; Roth, S.; et al. Raman spectrum of graphene and graphene layers. *Phys. Rev. Lett.* **2006**, *97*, 187401. [CrossRef] [PubMed]
30. Gu, S.; Hsieh, C.-T.; Gandomi, Y.A.; Chang, J.-K.; Li, J.; Li, J.; Zhang, H.; Guo, Q.; Lau, K.C.; Pandey, R. Microwave growth and tunable photoluminescence of nitrogen-doped graphene and carbon nitride quantum dots. *J. Mater. Chem. C* **2019**, *7*, 5468–5476. [CrossRef]
31. Vercelli, B.; Donnini, R.; Ghezzi, F.; Sansonetti, A.; Giovanella, U.; La Ferla, B. Nitrogen-doped carbon quantum dots obtained hydrothermally from citric acid and urea: The role of the specific nitrogen centers in their electrochemical and optical responses. *Electrochim. Acta* **2021**, *387*, 138557. [CrossRef]
32. Ratsos, S.; Walke, P.R.; Mikli, V.; Ločs, J.; Šmits, K.; Vítola, V.; Šutka, A.; Kruusenberg, I. CO₂ turned into a nitrogen doped carbon catalyst for fuel cells and metal-air battery applications. *Green Chem.* **2021**, *23*, 4435–4445. [CrossRef]
33. Bite, I.; Laganovska, K.; Vanags, E.; Vitola, V. Synthesis and characterization of translucent hafnia ceramics. *Materialia* **2023**, *32*, 101887. [CrossRef]
34. Ferrari, A.C.; Basko, D.M. Raman spectroscopy as a versatile tool for studying the properties of graphene. *Nat. Nanotechnol.* **2013**, *8*, 235–246. [CrossRef] [PubMed]
35. Ferrari, A.C. Raman spectroscopy of graphene and graphite: Disorder, electron–phonon coupling, doping and nonadiabatic effects. *Solid State Commun.* **2007**, *143*, 47–57. [CrossRef]
36. Jorio, A.; Cançado, L.G.; Malard, L.M. Vibrations in Graphene. In *2D Materials*; Avouris, P., Heinz, T.F., Low, T., Eds.; Cambridge University Press: Cambridge, UK, 2017; pp. 71–89. [CrossRef]
37. Wall, M. The Raman Spectroscopy of Graphene and the Determination of Layer Thickness. Available online: <https://www.semanticscholar.org/paper/The-Raman-Spectroscopy-of-Graphene-and-the-of-Layer-Wall/b694948998d242c3a1361ec46a1d271ffee8e95c> (accessed on 2 June 2022).
38. Ratha, S.; Samantara, A.K. *Characterization and Performance Evaluation of Supercapacitor*; Springer: Singapore, 2018; pp. 23–43. [CrossRef]
39. Liu, C.; Yu, Z.; Neff, D.; Zhamu, A.; Jang, B.Z. Graphene-Based Supercapacitor with an Ultrahigh Energy Density. *Nano Lett.* **2010**, *10*, 4863–4868. [CrossRef] [PubMed]
40. Salunkhe, R.R.; Lee, Y.; Chang, K.; Li, J.; Simon, P.; Tang, J.; Torad, N.L.; Hu, C.; Yamauchi, Y. Nanoarchitected Graphene-Based Supercapacitors for Next-Generation Energy-Storage Applications. *Chem. Eur. J.* **2014**, *20*, 13838–13852. [CrossRef]
41. Chee, W.K.; Lim, H.N.; Zainal, Z.; Huang, N.M.; Harrison, I.; Andou, Y. Flexible Graphene-Based Supercapacitors: A Review. *J. Phys. Chem. C* **2016**, *120*, 4153–4172. [CrossRef]
42. Ren, X.; Meng, N.; Ventura, L.; Goutianos, S.; Barbieri, E.; Zhang, H.; Yan, H.; Reece, M.J.; Bilotti, E. Ultra-high energy density integrated polymer dielectric capacitors. *J. Mater. Chem. A* **2022**, *10*, 10171–10180. [CrossRef]
43. Hsia, B. *Materials Synthesis and Characterization for Micro-Supercapacitor Applications*; University of California: Berkeley, CA, USA, 2013; Available online: <https://escholarship.org/uc/item/8gn9b880> (accessed on 5 June 2022).
44. Gittins, J.W.; Chen, Y.; Arnold, S.; Augustyn, V.; Balducci, A.; Brousse, T.; Frackowiak, E.; Gómez-Romero, P.; Kanwade, A.; Köps, L.; et al. Interlaboratory study assessing the analysis of supercapacitor electrochemistry data. *J. Power Sources* **2023**, *585*, 233637. [CrossRef]
45. Conway, B.E. *Electrochemical Supercapacitors*; Springer: New York, NY, USA, 1999. [CrossRef]
46. Su, Y.; Xue, H.; Fu, Y.; Chen, S.; Li, Z.; Li, L.; Knoks, A.; Bogdanova, O.; Lesničenoks, P.; Palmbahs, R.; et al. Monolithic Fabrication of Metal-Free On-Paper Self-Charging Power Systems. *Adv. Funct. Mater.* **2024**, *34*, 2313506. [CrossRef]

Disclaimer/Publisher’s Note: The statements, opinions and data contained in all publications are solely those of the individual author(s) and contributor(s) and not of MDPI and/or the editor(s). MDPI and/or the editor(s) disclaim responsibility for any injury to people or property resulting from any ideas, methods, instructions or products referred to in the content.